Plasmonic black absorbers for enhanced photocurrent of visible-light photocatalysis

Furui Tan,[a,b] Ning Wang,[a,b] Dang Yuan Lei,[a,b] Weixing Yu[c] and Xuming Zhang*[,a,b]

[a] The Hong Kong Polytechnic University Shenzhen Research Institute, Shenzhen, China 518057

[b] Department of Applied Physics, The Hong Kong Polytechnic University, Hong Kong, China

[c] Key Laboratory of Spectral Imaging Technology, Xi'an Institute of Optics and Precision Mechanics, Chinese Academy of Sciences, Xi'an, China 710119.

E-mail: apzhang@polyu.edu.hk

Abstract

Plasmonic resonance of noble metal nanoparticles can drastically enhance the visible response of wide-bandgap photocatalysts like TiO_2, but the current technology has two fundamental problems: narrow absorption band and low absorption, which limit the energy efficiency of photocatalysis using sunlight. Here we report an original work of plasmonic black absorber that sandwiches a 150-nm TiO_2 layer between a layer of random Au nanoparticles and a rough Au surface (200 nm thick). The combined plasmonic effect of the Au nanoparticles and the Au rough surface enables a strong absorption (72% – 91%) over 400 – 900 nm and a significantly enhanced photocurrent (by 20 folds) as compared to the bare TiO_2 film. The strong absorption to visible and near infrared light, and the much enhanced photocurrent make the black absorber an ideal material for solar applications such as photocatalytic, photosynthetic, photovoltaic and photothermal systems.

Keywords: plasmonics, black absorbers, photocatalysis, perfect absorbers, solar energy

26

27

1. Introduction

As an abundant and irreplaceable resource, solar energy has been intensively exploited for human activities. Photocatalysis utilizes semiconductors to transform photon energy into chemical energy by absorbing photons and generating electrons without harmful byproduct.[1],[2],[3] Although TiO_2 is the most promising photocatalyst thanks to its many merits such as superior photoactivity, high photostability, proven biosafety and abundant supply, it has its own Achilles' heel – the wide bandgap (~3.2 eV). This limits its absorption to only the UV light (< ~ 388 nm), making it absorb only about ~ 4% of solar energy. Many attempts have been made to enhance the response of TiO_2 to the visible light and even the near infrared light. Among them, doping of non-metallic elements such as nitrogen,[4],[5] carbon,[6],[7] and sulphur,[8],[9] have attracted much attention, however, the doped TiO_2 photocatalysts are often not stable enough.

Recently, plasmonic photocatalysis has risen up as a very promising technology for high-performance photocatalysis.[10],[11] It involves dispersal of noble metal nanoparticles (NPs) (commonly Au NPs and Ag NPs in the sizes of tens to hundreds of nanometers) into semiconductor photocatalysts by either dispensing on the surface or embedded in the semiconductors.[12],[13],[14] The localized surface plasmonic resonance (LSPR) effect of noble metal NPs enables it to absorb the visible light and transfer the energy to TiO_2 for photocatalysis.[15],[16],[17],[18] Nevertheless, the LSPR effect has two fundamental limits. One is that the resonant effect limits its absorption bandwidth to a narrow wavelength range (typically ~ 50 nm or smaller for uniform nanospheres).[18] The other is that the absorption coefficient is usually low due to the strong scattering. To shift the LSPR resonance to the visible range, the size of NPs has to be large (~ 50 – 100 nm) and thus the scattering becomes prominent. For instance, the Au nanosphere with the diameter of 80 nm has the resonance wavelength at 550 nm, but its scattering coefficient is already 0.65 of the absorption coefficient.[19] And larger nanospheres shift the resonance peak to longer wavelength, but at

the cost of larger scattering. Although the scattering may contribute to the photocurrent by increasing the photon-photocatalyst interaction length,[11] it is more desirable to have photons strongly absorbed by the NPs, especially when the photon energy is lower than the bandgap of photocatalyst materials (e.g., visible light to TiO_2). Therefore, a blackbody-like absorber would be ideal to make full use of the whole solar spectrum.[20],[21],[22],[23],[24] Recently, blackbody-like metallic layers in the form of diffraction grating have been reported for strong absorption over a wide wavelength.[25] Special efforts have been made to enhance the absorption to the infrared light as well.[26],[27],[28] However, those man-made regular nanostructures are often polarization dependent and involve complicated photolithographic processes. Recently, a broadband plasmonic-metamaterial absorber was reported using a three-layer metallo−dielectric−metallo stack.[29] The top layer is a very thin discontinuous Au layer (7 nm thick), the middle layer is a thin SiO_2 layer (40 nm thick) and the bottom is a flat Au film (100 nm thick). Although this approach promises easy fabrication and excellent absorption in visible-light range, this work focused only on the broadband absorption. In addition, the non-conductivity of SiO_2 layer blocks the electron transportation, making it not suitable for photocurrent-based applications like the photocatalysis.

In this paper, we demonstrate a new black absorber structure using TiO_2 as the dielectric medium. This unique black absorber based on the plasmonic effect of random Au nanostructures, which exhibits strong absorption (> 70%) of non-coherent sunlight over 400 – 900 nm and overcomes the major problems of current LSPR-based photocatalysis technology. The absorber is composed of a TiO_2 layer sandwiched between a layer of Au nanoparticles (AuNPs) and a rough Au layer (in short, AuNP/TiO_2-Au film). For comparison, another three structures such as the bare TiO_2 film, the AuNPs on TiO_2 layer (named as AuNP/TiO_2 hereafter) and the TiO_2 layer on Au layer (named as TiO_2-Au film) are developed as well. Experiments will be conducted to prove that the black absorber has apparently superior photocatalytic performance than the other three structures, and simulations will be carried out

to show the origin of strong absorption. It is worth noting that the fabrication involves only simple processes, such as sputtering and annealing, and requires no photopatterns, making it easy to fabricate large-area samples at low cost.

2. Results and discussion

2.1 Layer structure

From top to bottom, the structure of black absorber consists of a layer of randomly distributed AuNPs as the plasmonic absorber, a TiO_2 thin layer as the photocatalyst and a layer of rough Au layer as another plasmonic absorber (see Figure 1a). To lead out the photocurrent, the rough Au layer sits on a glass substrate coated with a transparent conducting FTO film. To enhance the adhesion between the FTO film and the rough Au layer, a thin chromium layer is coated. Figure 1b shows the three-terminal potentiostat setup for the measurement of photocurrent in the KOH solution. The black absorber acts as the working electrode, a platinum plate as the counter-electrode and a saturated cell as the reference electrode. Figure 1c exemplifies the working principle. The rough Au layer absorbs photons of various energies to generate hot electrons, which are fed into the TiO_2 layer.[30],[31] The AuNPs serve mainly two functions, an electron trap and an LSPR absorber. As the electron trap, the AuNPs accumulates the hot electrons from the TiO_2 layer and also provides a fast lane for the transfer of electrons to the electrolyte.[32] As the LSPR absorber, the AuNPs assist the absorption of the photons of its own LSPR wavelength and contributes to the photocatalysis as well. In this manner, the Au rough layer and the AuNPs work together to absorb a broad range of visible and near-infrared light in the solar light.

2.2 Micrographs

Figure 2a shows the pseudo-color SEMs of the cross-section of the plasmonic black absorber. For the Au layer and the TiO_2 layer, large grains can be observed and their

boundary is not straight and not clear. In fact, they have partial overlap along the boundary and form effectively a thin Au-TiO_2 composite layer, which ensures good physical contact for the transport of photo-excited electrons from the Au layer to the TiO_2 layer. It is interesting to see that most of the TiO_2 gains run continuously along the vertical direction, which is beneficial to the charge transfer across the TiO_2 layer. Thicknesses of the Au layer and the TiO_2 layer are about 200 nm and 150 nm, respectively. It is noted that the Au layer is thick enough to block all incidence light and thus the transmission becomes negligible. The AuNPs on the surface of TiO_2 layer are fabricated by the sputtering and annealing method. Particle sizes are controlled by the deposition thickness of Au and the annealing conditions. From Figure 2b, most of the AuNPs are well dispersed. The histogram shows the size of AuNPs mainly ranges from 40 to 100 nm, and is mostly at 70 nm (see Supporting Information, Figure S2). Fig. 2c show the typical morphology of the interlayer TiO_2, which is uniform and continuous. A thin Au-TiO_2 composition layer forms at the boundary. Figure 2d shows the top-views of the Au layer (by etching a window in the TiO_2 layer). The Au layer is very rough, with dense nano-cavities (or nanopores) and Au nanostructures of varying geometries. The average roughness is 11.0 nm (see Supporting Information, Figure S3). Such a rough surface of the Au layer is the key to the broad absorption due to the plasmonic effects of the nano-cavities and the Au nanostructures and their coupling effect. [20],[21],[22],[33],[34]

2.3 Optical absorption spectra

Figure 3 plots the absorption spectrum of the black absorber (i.e., AuNP/TiO_2-Au film) as compared with those of the bare TiO_2 film, the AuNP/TiO_2 film and the TiO_2-Au film. Here the absorption A is calculated by the equation $A = 1 - R - T$, where R and T are the normalized reflection and transmission, respectively. The insets of Figure 3 show the corresponding photos under the UV cut-off solar light ($\lambda > 400$ nm). The bare TiO_2 film looks pale white under sunlight and has very low absorption. For the TiO_2 layer that are loaded only

with AuNPs (i.e., the AuNP/TiO_2 film), it shows a color of light pink (see the inset of Figure 3). The spectrum has an absorption peak at around 560 nm but the absorption coefficient is still low (< 15%). The absorption peak can be ascribed to the LSPR excitation effect of the AuNPs. For the TiO_2-Au film, its photo becomes dark brown, and the absorption coefficient is significantly increased (> 50%) over the whole range of 400 – 900 nm. This is an evidence of high absorption of the rough Au layer, though there is a valley of absorption near 600 nm. It is particularly interesting to see that the absorption rises up when the wavelength is > 600 nm. This is opposite to most of the photocatalysts that use uniform noble metal NPs, whose absorption often drops significantly for the long wavelength part of visible light and the near-infrared region.[35] This feature can be regarded as a spectral signature of the black absorbers.[23] For the AuNP/TiO_2-Au film of our research focus, the absorption coefficient is further enhanced to > 72% over 400 – 900 nm. Particularly, a peak absorption of 91% appears at ~ 600 nm, thanks to the LSPR absorption of AuNPs.[36],[37] It is worth highlighting that the photo of the sample shows a deep dark color (see the inset of Figure 3), well proving its likeness to "blackbody". For the colors of different samples, the pale white color of the bare TiO_2 film is attributed to its low and quite flat absorption in 450 – 750 nm; the pink appearance of the AuNP/TiO_2 film is rendered by its relatively higher absorption in short wavelength region in 400 – 550 nm; the brown color of the TiO_2-Au film is owning to the drop of absorption in 500 – 650 nm; and the dark color of the AuNP/TiO_2-Au film is a result of the very high absorption over the whole range of 400 – 900 nm.

2.4 Photoelectrochemical properties

To study the photo-induced charge separation, the photoelectrochemical (PEC) properties of the bare TiO_2 film, the AuNP/TiO_2 film, the AuNP/TiO_2-Au film and the TiO_2-Au film are tested under the on-off illumination of a broadband visible source (400 – 900 nm, ~50 mW/cm^2) using the setup as shown in Figure 1b. The linear sweep voltammograms (LSV) are

158 performed both in dark and under visible-light illumination (see Figure 4a), which reveals an
159 apparent response to light on/off switching at different bias potentials. The chopped *I-t* curves
160 are measured and recorded at a constant potential of 0 V (see Figure 4b), which is in good
161 agreement with the *I-V* curves at 0 V bias voltage. Clearly, the bare TiO_2 produced little
162 photocurrent density, < 0.7 μA cm^{-2}, which is just above the background dark current. As
163 expected, a significant photocurrent density enhancement is observed on the AuNP/TiO_2-Au
164 film (i.e., the black absorber), with a photocurrent density of ~15 μA·cm^{-2} (take the values at
165 90 s). The enhancement factor is ~ 20 as compared to the bare TiO_2 film. The TiO_2-Au film
166 enhances the photocurrent density to ~ 5 μA·cm^{-2} in the absence of AuNPs loading, yielding
167 an enhancement factor of ~ 8 with respect to that of the bare TiO_2. On the other hand, the
168 addition of AuNPs onto the TiO_2 layer has just doubled the photocurrent in the absence of Au
169 layer. Generally, the magnitude of photocurrent follows the AuNP/TiO_2-Au film > the TiO_2-
170 Au film > the AuNP/TiO_2 film > the bare TiO_2 film, which is in good agreement with the
171 order of absorption spectra in Figure 3. The large photocurrent of the AuNP/TiO_2-Au film as
172 compared to that of the TiO_2-Au film is attribute to the fast-lane transfer and the LSPR
173 absorption of the AuNPs as explained above. For the AuNP/TiO_2 film, its photocurrent is very
174 small as compared to the AuNP/TiO_2-Au film, owing to the low absorption ability as seen in
175 Figure 3. Regarding to the influence of the layer thicknesses in the AuNP/TiO_2-Au film, it is
176 found that the current combination (i.e., 200 nm thick for the Au layer and 150 nm for the
177 TiO_2 layer) yields the best absorption spectrum and the highest photocurrent; a thicker or
178 thinner Au layer would reduce the level of absorption coefficient and the flatness of the
179 absorption spectrum; similarly, a thinner TiO_2 layer causes a reduction of absorption but a
180 thicker TiO_2 layer lowers the photocurrent slightly, possibly due to the larger grain size and
181 the longer transport distance of electron from the Au layer to the electrolyte. For the origins of
182 photocurrents in the AuNP/TiO_2-Au film and the TiO_2-Au film, the contribution of hot

electrons can be inferred from the corresponding chopped I-V curves in Figure 4a and the I-t plots in Figure 4b: their values are positive in the circuit connection of Figure 1c, showing that the electrons flow from the rough Au layer to the TiO_2 layer and then to the electrolyte; the photon energy (3.1 – 1.4 eV for the wavelength 400 – 900 nm) is lower than the TiO_2 bandgap (~ 3.2 eV) and thus the photo-generated electrons have to result from the plasmonic resonance of Au nanostructures of the rough Au films. The contribution of hot electrons to photocurrent has been extensively used in the TiO_2 films sensitized by the AuNPs[30],[31], it is reasonable to apply the similar mechanism to the rough Au films of this work.

The incident photons to current conversion efficiency (IPCE) expresses the number of electrons per unit number of incident photons at a given irradiation wavelength. Figure 4c displays the photocurrent vs. wavelength curves, which are measured by using the bandpass filters (bandwidth 20 nm, central wavelengths at 425, 450, 475, 500, 520, 550, 600 and 650 nm, respectively). For all the four TiO_2-based samples, the photocurrent peaks appear at 450 nm. Figure 4d plots the IPCE vs. wavelength curves that are calculated from the PEC data in Figure 4c according to the formula

$$\mathrm{IPCE}(\%) = (1240 \times I_{sc}) / (\lambda \times P_{light}) \times 100$$

where λ is the wavelength of the incident light, P_{light} is the illumination power density at the specific wavelength and I_{sc} is the measured short circuit photocurrent density at the specific wavelength. It is seen that the IPCE value drops quickly in 424 – 475 nm and then becomes flat at longer wavelengths. Nevertheless, the use of Au NPs or Au film leads to an increase of IPCE over the wide visible range, and the AuNP/TiO_2-Au film presents the highest IPCE, which is consistent with the absorption spectra. At wavelengths shorter than 550 nm, the AuNP/TiO_2-Au film presents much higher IPCE values compared to the AuNP/TiO_2 film photoelectrode, indicating that the high IPCE is mainly attributed to the presence of the rough Au film rather than Au NPs.

2.5 Numerical simulation

Finite-difference time-domain (FDTD) simulations are carried out to calculate the absorption spectra of the AuNP/TiO_2-Au film using a commercial software package, Lumerical FDTD Solutions.[38],[39] Here, we will investigate the electromagnetic response of the AuNP/TiO_2-Au film under visible light and will compare it with the measured spectrum. The perspective view of the structure and the cross-sectional view in the *xz* plane ($y = 0$) are showed in Figure 5a and 5b, respectively. In the simulation, the physical structures, from bottom to top, are represented by five layers: *Layer A*, a continuous Au layer at the bottom (200 nm thick); *Layer B*, a layer of random Au particles (represented by 3,000 AuNPs with the size randomly distributed in 20 – 40 nm); *Layer C*, a TiO_2 layer (150 nm thick); *Layer D*, a TiO_2-Au particle composite (800 random TiO_2 particles in 40 – 60 nm); and *Layer E*, another layer of Au nanoparticles (300 AuNPs in 20 – 100 nm). These layers are chosen to resemble the real structures of the AuNP/TiO_2-Au film (see Figure 2a) as much as possible but using only simple structures like films and nanospheres. More details of simulation will be described in Methods Section.

Figure 5c plots the simulated absorption spectrum of the AuNP/TiO_2-Au film. It resembles closely the shape of measured spectrum over the whole range of 400 – 900 nm. Particularly, the positions of the absorption peak and two valleys given by the simulation align well with those by the experiment. Nevertheless, the simulation shows higher absorption coefficient at the peak than the experiment, which is probably ascribed to the imperfections of using the five simple layers to represent the real structure.

The field enhancement is further confirmed by the 3D FDTD software. From the simulation curve in Figure 5c, the absorption reaches the minimum at 500 nm (77%) and 700 nm (70%), and the maximum at 410 nm (97%) and 600 nm (95%). Therefore, the wavelengths of 410, 500, 600, 700, 800 and 900 nm are chosen as the working wavelengths to simulate the electric field intensity distribution in the *xz* plane. As shown in Figure 6a, the

electric field intensity is enhanced in two random Au particle layers, Layer B and E, though Layer E has a greater enhancement. In Figure 6b and 6d that have λ = 500 nm and 700 nm, the electric fields in Layer E are reduced, showing a low contribution from the AuNPs. This corresponds to the absorption valleys at 500 nm and 700 nm in Figure 5c. In Figure 6c that has λ = 600 nm, the electric field in Layer E becomes apparent again, indicating a strong absorption of the AuNPs due to the LSPR effect. This corresponds to the absorption peak at 600 nm in Figure 5c. In Figure 6e and 6f, only Layer B shows strong electric field. Based on Figure 6a-f, it can be observed that the rough Au layer (Layer B) always has intense electric field and becomes dominant when the wavelength is apart from the plasmonic resonant wavelength of AuNPs (λ = 600 nm). This proves that the rough Au surface always has strong plasmonic absorption over 400 – 900 nm and the AuNPs mainly contribute to the LSPR absorption at 600 nm. In the other word, the blackbody-like absorption is a combination of the plasmonic absorptions of the rough Au layer and the AuNPs.

3. Conclusions

In summary, an original study on the plasmonic black absorber is demonstrated using the sandwiched structure that comprises a layer of AuNPs, a TiO_2 layer and a rough Au layer. It obtains an excellent absorption over the range of 400 – 900 nm due to the combined plasmonic absorptions of the rough Au layer and the AuNPs as verified by the FDTD simulation. By transferring hot electrons to the TiO_2 layer, the black absorber is able to enhance the photocurrent by 20 folds as compared to the bare TiO_2 under the UV cut-off solar light (> 400 nm). Such an absorber is simple, easy to fabricate and superior to other plasmonic materials. Its broadband strong absorption of the visible and near infrared light is particularly favorable for the photocatalysis using sunlight and would find potential applications in water splitting, environmental remediation and photosyntheses.

4. Experimental

4.1 Fabrication

The plasmonic black absorber and all the other films are fabricated on the substrate of fluorine-doped tin oxide (FTO) glass. First, a thin Cr layer (~ 10 nm thick) and a continuous Au layer (~ 200 nm thick) are deposited by magnetron sputtering on the FTO substrate. The working pressure of Ar and the sputtering power are 6 pa and 60 W, respectively. The layer thicknesses are controlled by the sputtering time. The Cr layer is to enhance the adhesion and the electrical conduction of the Au layer to the FTO substrate.

Then, the TiO_2 layer is deposited by the spin-coating method. It starts with the preparation of TiO_2 sol-gel. Titanium isopropoxide (TIP) $Ti[OCH(CH_3)_2]_4$ with purity 98% is introduced as the source of titanium and 2.5-ml diethanolamine $\{HO(CH_2)\}_2NH$ is dissolved in 70-ml ethanol (CH_3CH_2OH) with the purity of 99.7%. The mixture is sealed and stirred at 40 ^oC for 20 min with a magnetic stirrer. After adding the precursor of 9-ml TIP to the water-free mixture, the stirring process is continued for another 20 min. When a slightly yellow and transparent gel is formed, 20-ml water and 1-ml ethanol are added into the gel and stirred for another 20 min. The obtained solution is kept at ambient temperature for 24 h. After the sol-gel is ready, it is spin-coated onto the Au layer with a spinning speed of 2000 rpm for 30 s. The obtained TiO_2 layer is sintered at 500 ^oC in air for 1 h to get the anatase phase. Although the annealing temperature of 500 ^oC is pretty high and may cause the oxidation problem, previous studies and our experience show that stable Au films and Au nanoparticles can still be obtained safely.

Finally, sputtering and thermal annealing are utilized to fabricate the random distribution of AuNPs onto the surface of TiO_2 layer. Here a thin Au layer is deposited by magnetron sputtering. After being annealed at 500 ^oC for 1 h, the thin Au layer is transformed into AuNPs during the annealing-cooling process.[33] The obtained AuNPs are mostly

spherical but with random sizes. The Au layers deposited for different sputtering times (and thus different thicknesses, in the range of 3 – 25 nm) result in the AuNPs of different sizes. The photos and the scanning electron micrographs (SEM) are shown in Supporting Information, Figure S1. When the Au layer is deposited onto the TiO_2 layer for 10 s, the AuNPs after annealing have the size in the range of 40 – 80 nm, as shown in Supporting Information, Figure S2.

4.2 Characterization

The surface morphology and the cross-section of the plasmonic blackbody-like structure are evaluated by the scanning electron microscope (Hitachi S-4800, Hitachi High-Technologies Corporation, Tokyo, Japan) with a cold field emission electron source and an in-lens secondary detector. Typically, the images are acquired with an acceleration voltage of 5 kV. UV-Vis spectrophotometer (Perkin Elmer Lambda 750) is employed to measure the absorption of the black absorber and the other samples of control experiments. The reflection spectra are performed with an integrating sphere that uses a $BaSO_4$ plate as the reference. This means that both the direct reflected light and the diffuse scattering light are included in the reflection measurement. The photocurrent is characterized using a three-terminal potentiostat (Figure 1b). The black absorber, a Pt electrode and a saturated calomel electrode (SCE) are used as the working, the counter, and the reference electrode, respectively. The working electrode potential is set at 0 V versus SCE. Photocurrent is measured under the irradiation of a Xe lamp (100 mw/cm^2) fixed with a UV filter (cut-off wavelength 400 nm).

4.3 FDTD simulation

To model the complicated structure, the AuNP/TiO_2-Au film is simplified into five layers. More specifically, Layers A and B represent the continuous part and the rough surface of the Au layer, respectively; Layer C stands for the continuous part of the TiO_2 layer; Layer D

represents the overlapping of the TiO_2 rough surface and the AuNPs; and Layer E represents the independent AuNPs on the surface of TiO_2. The 3D FDTD has been performed in a domain of 1 μm × 1 μm × 100 nm. For Layer A, the Au layer is 100 nm thick. For Layer B, it is represented by 3000 AuNPs with the size randomly distributed in 20 – 40 nm. For Layer C, the TiO_2 layer is 100 nm thick. For Layer D, it is represented by 800 random TiO_2 particles with the diameter in 40 – 60 nm. For Layer E, it contains 300 AuNPs with the size in 20 – 100 nm, following the histogram in Supporting Information, Figure S2b.

In the 3D FDTD simulation using Lumerical FDTD Solutions, the periodic boundary conditions are employed in both *x* and *y* directions, and the perfectly matched layer (PML) boundary condition is employed in the *z* direction. Although the distribution of random particles is not periodic, the periodicity of the unit cell in both the *x* and *y* directions are set as 1000 nm, which is far greater than the radius of the random particles to simulate the rough Au surface in the real structure. The FDTD lattice is completed with the auto non-uniform mesh type, the 6th level with the mesh type of high accuracy to ensure reliable results.

The absorption is calculated by the equation $A(\lambda) = 1–R(\lambda)–T(\lambda)$, where $R(\lambda) = |S_{11}|^2$ is the reflection and $T(\lambda) = |S_{21}|^2$ is the transmission. Since the bottom Au layer (thickness 160 nm) is much thicker than its typical skin depth, there is almost no transmission in the whole wavelength range, i.e. $T(\lambda) = 0$. In this case, the formulation of absorption can be simplified into $A(\lambda) = 1 – R(\lambda)$. Frequency-domain field and power monitor are used to investigate the S-parameters of transmission (S_{21}) and reflection (S_{11}) of a single unite cell.

Supporting Information

Supporting Information is available from the Wiley Online Library or from the author.

Acknowledgements

This work is supported by National Natural Science Foundation of China (no. 61377068), Research Grants Council of Hong Kong (N_PolyU505/13, PolyU 5334/12E, PolyU 152184/15E, and 509513), and The Hong Kong Polytechnic University (grants G-YN07, G-YBBE, 4-BCAL, 1-ZVAW, 1-ZE14, A-PM21, 1-ZE27 and 1-ZVGH).

REFERENCES

[1] W. Hou, S. B. Cronin, *Adv. Funct. Mater.* **2013**, *23*, 1612.

[2] A. Primo, A. Corma, H. García, *Phys. Chem. Chem. Phys.* **2011**, *13*, 886.

[3] X. Zhang, Y. L. Chen, R.-S. Liu, D. P. Tsai, *Rep. Prog. Phys.* **2013**, *76*, 046401.

[4] R. Asahi, T. Morikawa, T. Ohwaki, K. Aoki, Y. Taga, *Science* **2001**, *293*, 269.

[5] H. Irie, Y. Watanabe, K. Hashimoto, *J. Phys. Chem. B* **2003**, *107*, 5483.

[6] H. Irie, Y. Watanabe, K. Hashimoto, *Chem. Lett.* **2003**, *32*, 772.

[7] K. Woan, G. Pyrgiotakis, W. Sigmund, *Adv. Mater.* **2009**, *21*, 2233.

[8] T. Umebayashi, T. Yamaki, S. Tanaka, K. Asai, *Chem. Lett.* **2003**, *32*, 330.

[9] T. Tachikawa, S. Tojo, K. Kawai, M. Endo, M. Fujitsuka, T. Ohno, K. Nishijima, Z. Miyamoto, T. Majima, *J. Phys. Chem. B* **2004**, *108*, 19299.

[10] A. Aubry, D. Y. Lei, A. I. Fernández-Domínguez, Y. Sonnefraud, S. A. Maier, J. B. Pendry, *Nano Lett.* **2010**, *10*, 2574.

[11] S. Linic, P. Christopher, D. B. Ingram, *Nat. Mater.* **2011**, *10*, 911.

[12] Y. C. Pu, G. Wang, K. Der Chang, Y. Ling, Y. K. Lin, B. C. Fitzmorris, C. M. Liu, X. Lu, Y. Tong, J. Z. Zhang, Y. J. Hsu, Y. Li, *Nano Lett.* **2013**, *13*, 3817.

[13] K. Awazu, M. Fujimaki, C. Rockstuhl, J. Tominaga, H. Murakami, Y. Ohki, N. Yoshida, T. Watanabe, *J. Am. Chem. Soc.* **2008**, *130*, 1676.

[14] S. Mubeen, G. Hernandez-Sosa, D. Moses, J. Lee, M. Moskovits, *Nano Lett.* **2011**, *11*, 5548.

[15] Y. Nishijima, K. Ueno, Y. Yokota, K. Murakoshi, H. Misawa, *J. Phys. Chem. Lett.* **2010**, *1*, 2031.

[16] D. Y. Lei, A. I. Fernández-Domínguez, Y. Sonnefraud, K. Appavoo, R. F. Haglund, J. B. Pendry, S. a. Maier, *ACS Nano* **2012**, *6*, 1380.

[17] A. Ji, R. P. Sharma, A. Kumari, N. K. Pathak, *Plasmonics* **2013**, *9*, 291.

[18] M. Hu, J. Chen, Z.-Y. Li, L. Au, G. V Hartland, X. Li, M. Marquez, Y. Xia, *Chem. Soc. Rev.* **2006**, *35*, 1084.

[19] K. Awazu, M. Fujimaki, C. Rockstuhl, J. Tominaga, H. Murakami, Y. Ohki, N. Yoshida, T. Watanabe, *J. Am. Chem. Soc.* **2008**, *130*, 1676.

[20] M. K. Hedayati, M. Javaherirahim, B. Mozooni, R. Abdelaziz, A. Tavassolizadeh, V. S. K. Chakravadhanula, V. Zaporojtchenko, T. Strunkus, F. Faupel, M. Elbahri, *Adv. Mater.* **2011**, *23*, 5410.

[21] V. G. Kravets, S. Neubeck, a. N. Grigorenko, a. F. Kravets, *B - Condens. Matter Mater. Phys.* **2010**, *81*, 1.

[22] Y. H. Lin, B. Händel, H. J. Huang, H. A. Chen, Y. F. Chen, H. N. Lin, D. P. Tsai, *Plasmonics* **2013**, *8*, 377.

[23] T. Søndergaard, S. M. Novikov, T. Holmgaard, R. L. Eriksen, J. Beermann, Z. Han, K. Pedersen, S. I. Bozhevolnyi, *Nat. Commun.* **2012**, *3*, 969.

[24] K. Mizuno, J. Ishii, H. Kishida, Y. Hayamizu, S. Yasuda, D. N. Futaba, M. Yumura, K. Hata, *Proc. Natl. Acad. Sci. U. S. A.* **2009**, *106*, 6044.

[25] V. G. Kravets, F. Schedin, a. N. Grigorenko, *Phys. Rev. B - Condens. Matter Mater. Phys.* **2008**, *78*, 97.

[26] X. Liu, T. Tyler, T. Starr, A. F. Starr, N. M. Jokerst, W. J. Padilla, *Phys. Rev. Lett.* **2011**, *107*, 4.

[27] N. Liu, M. Mesch, T. Weiss, M. Hentschel, H. Giessen, *Nano Lett.* **2010**, *10*, 2342.

[28] A. Moreau, C. Ciracì, J. J. Mock, R. T. Hill, Q. Wang, B. J. Wiley, A. Chilkoti, D. R. Smith, *Nature* **2012**, *492*, 86.

[29] Z. Liu, X. Liu, S. Huang, P. Pan, J. Chen, G. Liu, G. Gu, *ACS Appl. Mater. Interfaces* **2015**, *7*, 4962.

[30] Y. K. Lee, C. H. Jung, J. Park, H. Seo, G. A. Somorjai, J. Y. Park, *Nano Lett.* **2011**, *11*, 4251.

[31] J. Y. Park, L. R. Baker, G. A. Somorjai, *Chem. Rev.* **2015**, *115*, 2781.

[32] C. Clavero, *Nat. Photonics* **2014**, *8*, 95.

[33] M. A. Nazirzadeh, F. B. Atar, B. B. Turgut, A. K. Okyay, *Sci. Rep.* **2014**, *4*, 7103.

[34] J. Lehman, E. Theocharous, G. Eppeldauer, C. Pannell, *Meas. Sci. Technol.* **2003**, *14*, 916.

[35] S. Linic, P. Christopher, D. B. Ingram, *Nat. Mater.* **2011**, *10*, 911.

[36] Z. Bian, T. Tachikawa, P. Zhang, M. Fujitsuka, T. Majima, *J. Am. Chem. Soc.* **2014**, *136*, 458.

[37] P. Englebienne, *Analyst* **1998**, *123*, 1599.

[38] E. Ozbay, *Science* **2006**, *311*, 189.

[39] A. Paris, A. Vaccari, A. C. Lesina, E. Serra, L. Calliari, *Plasmonics* **2012**, *7*, 525.

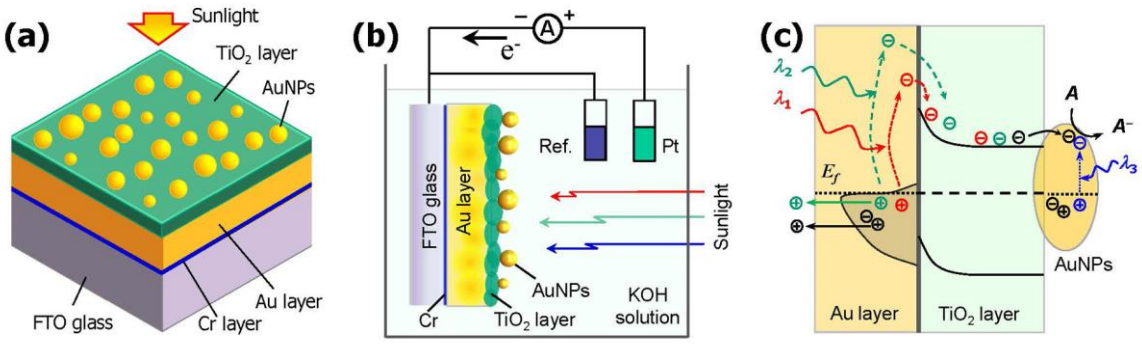

Figure 1 Plasmonic black absorber that is constructed by the AuNP/TiO2-Au film. (a) Layer structure. From bottom to top, it consists of a rough Au layer on the FTO glass substrate, a thin TiO_2 layer as the photocatalytic layer and a layer of Au nanoparticles on the top. (b) Three-terminal potentiostat setup for measuring the photocurrent of the perfect absorber. (c) Excitation and transfer of hot electrons in the absorber. The electrons flow from the Au layer toward the Au nanoparticles.

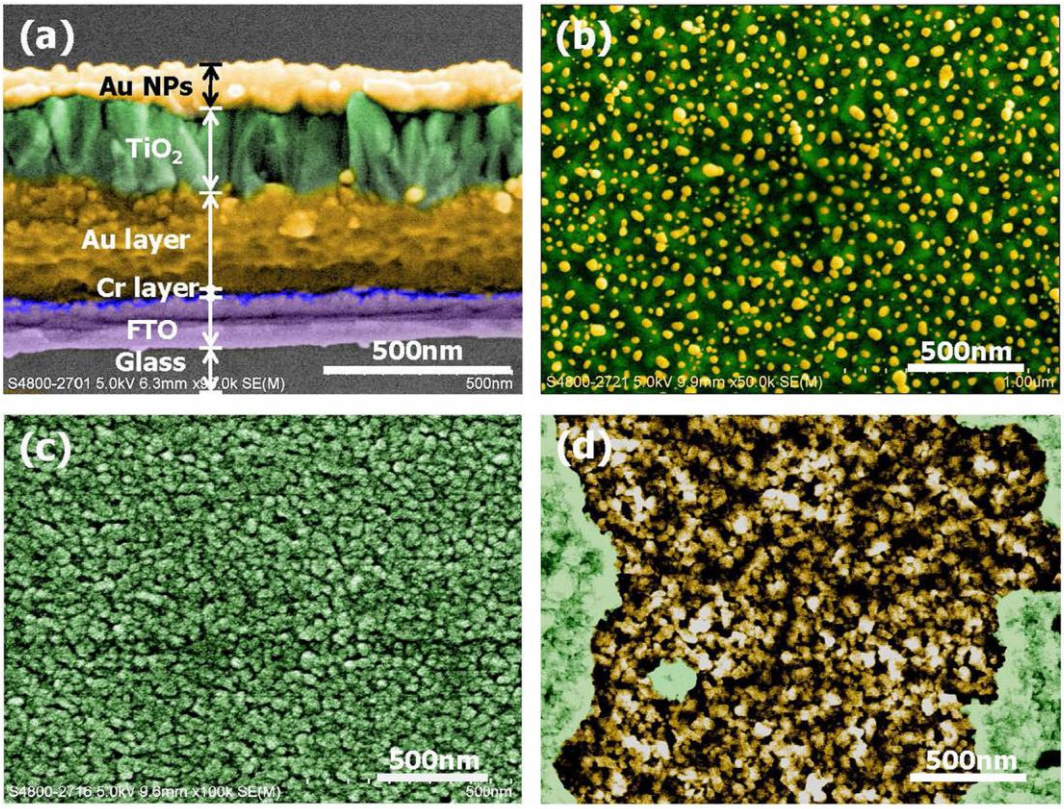

Figure 2 (a) Pseudo-color scanning electron micrograph of the cross-section of the absorber. The thicknesses of the Au layer and the TiO_2 layer are about 200 nm and 150 nm, respectively; and those of the FTO layer and the Cr layer are about 100 nm and 10 nm, respectively. (b) The Au nanoparticles on the top surface. (c) The TiO_2 film layer. (d) Top view of the Au layer exposed from an etched window of the TiO_2 layer, showing that the Au layer is very rough and consists of nanopores and nanoparticles.

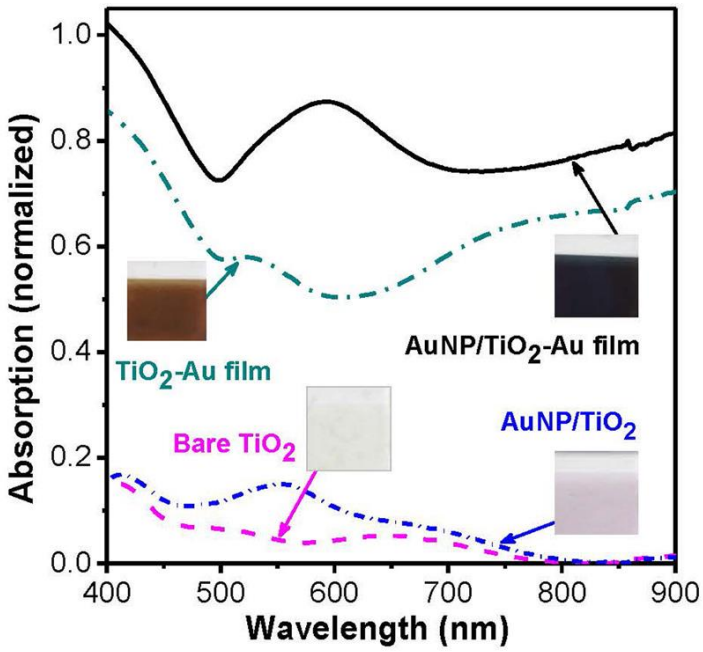

425

426 **Figure 3** The measured absorption spectra of different film samples. The insets show the
427 photos of the films. The bare TiO_2 film presents very low absorption, the AuNP/TiO_2 film has
428 also low absorption but a plasmonic absorption peak at ~560 nm, the TiO_2-Au film shows a
429 much enhanced absorption, where the AuNP/TiO_2-Au film exhibits strong absorption (> 72%)
430 over the whole range of 400 – 900 nm and the maximum absorption of 91% at ~600 nm.

431

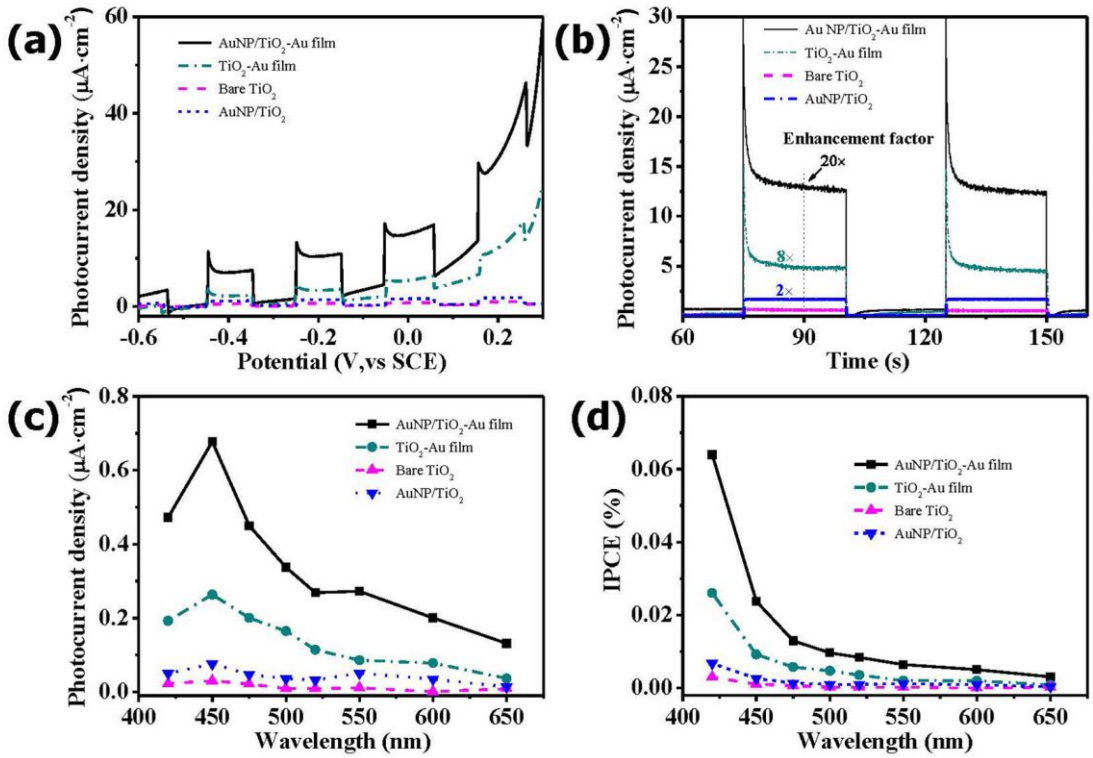

Figure 4 Comparisons of the photoelectrochemical properties of the four film samples. (a) Chopped *I-V* curves and (b) *I-t* plots under the irradiation of the UV cut-off solar light (with only $\lambda > 400$ nm). The photoelectrodes are measured versus the saturated calomel electrode (SCE) in the 1-M KOH solution. (c) Photocurrent action spectra and (d) the deduced IPCE spectra. In (b) – (d), the bias potential is kept at 0 V.

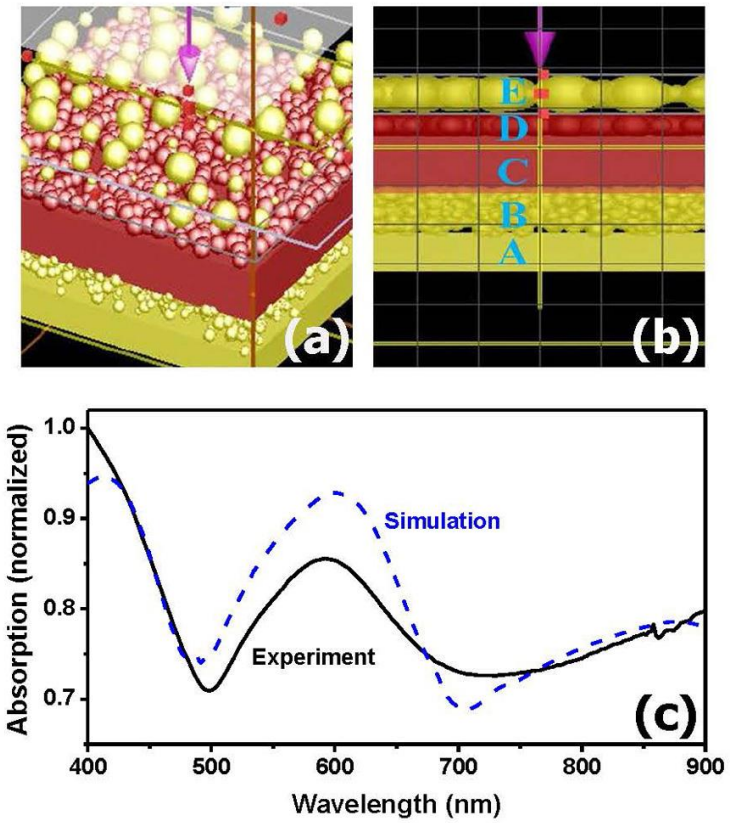

Figure 5 FDTD simulation. (a) Perspective view of the representative structure of black absorber for simulation. (b) Cross-sectional view in the *xz* plane. (c) Simulated absorption spectrum (blue dashed line) matches approximately the experimentally measured spectrum (black line).

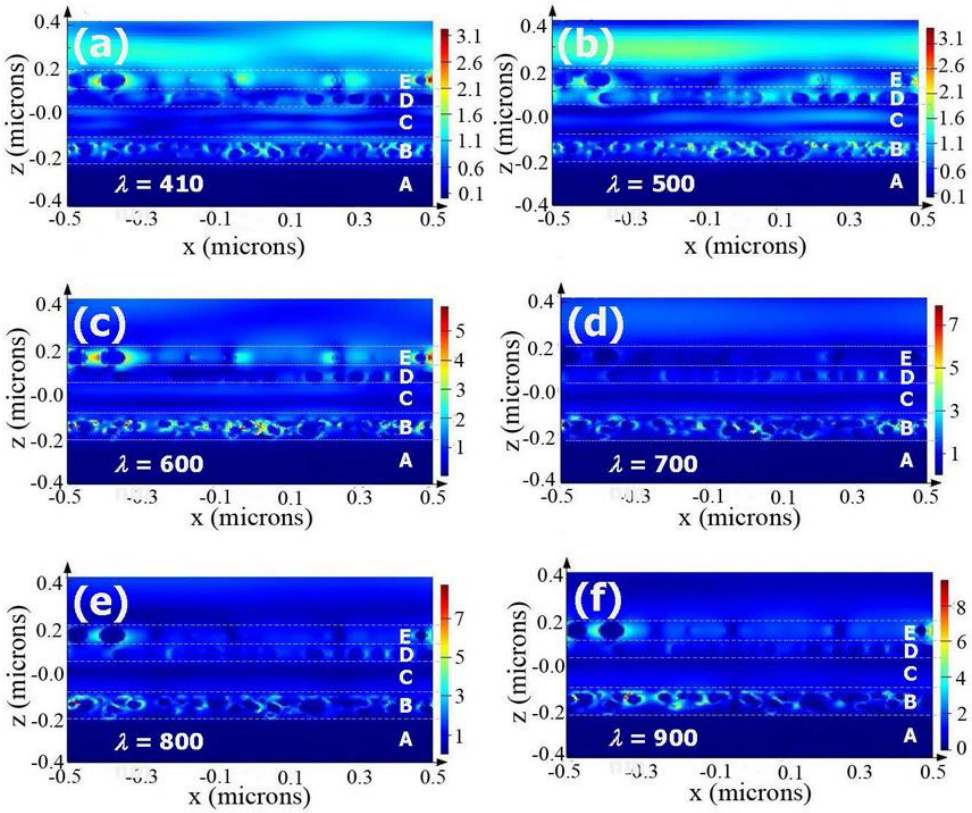

Figure 6 Distributions of electric field intensity for the perfect structure in the *xz* plane at six selected wavelengths: (a) 410 nm, (b) 500 nm, (c) 600 nm, (d) 700 nm, (e) 800 nm, and (f) 900 nm. The rough Au layer (i.e., Layer B) has always strong plasmonic resonance at different wavelengths and becomes the dominant absorber when the wavelength is longer than the plasmonic resonance wavelength 600 nm.

453 **Table of Contents**

454

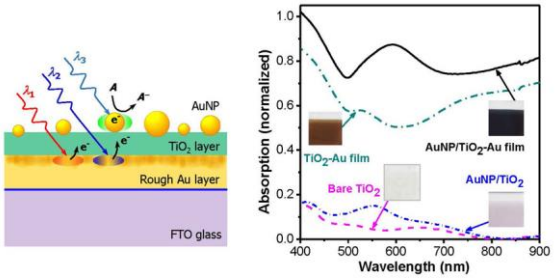

455

456

457 **To enhance the utilization of solar energy for photocatalysis,** the rough Au surface has
458 been combined with random Au nanoparticles to form a black absorber, which enables the
459 strong absorption (72% - 91%) to the solar light over 400 – 900 nm, and increases the
460 photocurrent by 20 folds. This black absorber represents an ideal material to enhance the
461 photocurrents in the solar applications such as photocatalytic, photovoltaic and photothermal
462 systems.

463

464

465

Plasmonic black absorbers for enhanced photocurrent of visible-light photocatalysis

Furui Tan,[a,b] Ning Wang,[a,b] Dangyuan Lei,[a,b] Weixing Yu[c] and Xuming Zhang*[,a,b]

[a] The Hong Kong Polytechnic University Shenzhen Research Institute, Shenzhen, China

[b] Department of Applied Physics, The Hong Kong Polytechnic University, Hong Kong, China

[c] Key Laboratory of Spectral Imaging Technology, Xi'an Institute of Optics and Precision Mechanics, Chinese Academy of Sciences, Xi'an, P. R. China.

E-mail: apzhang@polyu.edu.hk

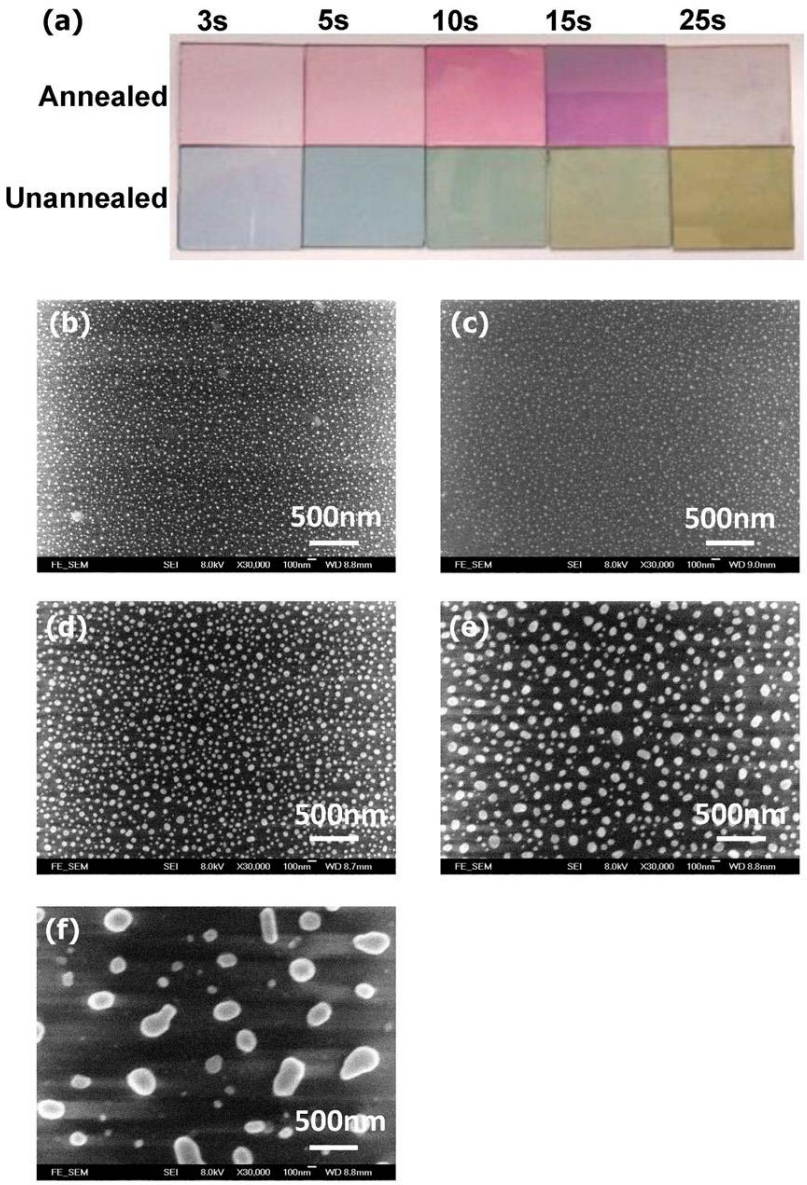

Figure S1. (a) Photographs of the Au films with the sputtering time of 3 s, 5 s, 10 s, 15 s and 25 s, before and after annealing at 500 ^{o}C; SEM images of the Au nanoparticles after annealing the Au films with the sputtering time of (b) 3 s; (c) 5 s; (d) 10 s; (e) 15 s and (f) 25 s. Before annealing, the colors of the Au films are deep. After annealing, the films turn to lighter color and are mostly pink. For the sizes of Au nanoparticles, they increase with longer deposition time.

485

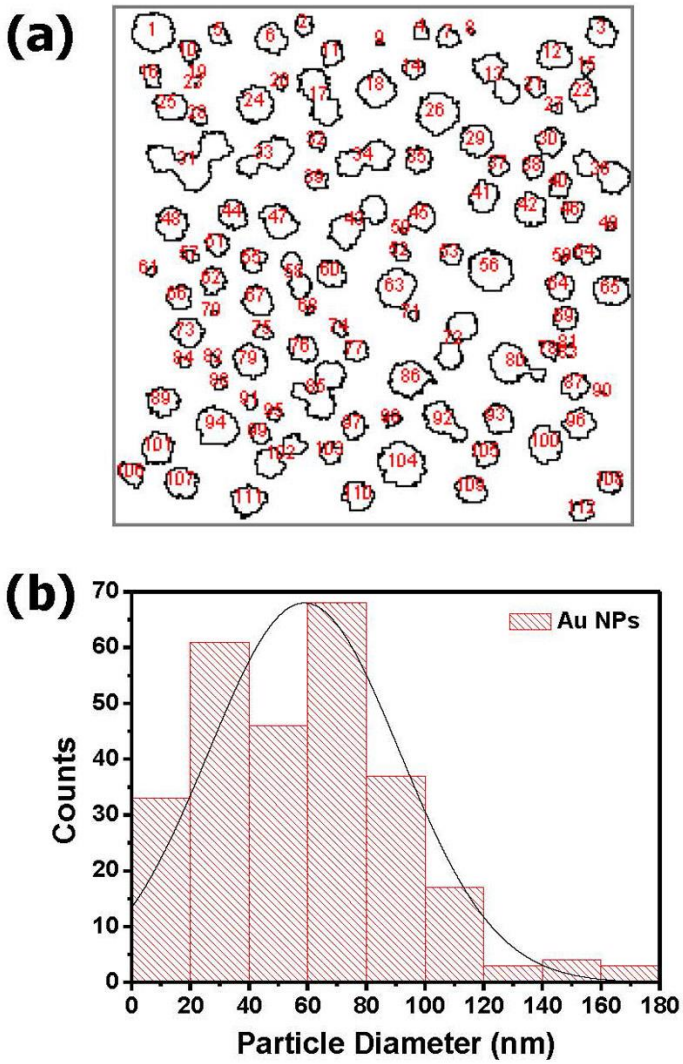

486

487 **Figure S2.** (a) Profile of Au nanoparticles in a small region of Fig. 2d. (b) Histogram of the

488 size of Au nanoparticles in Fig. 2d, as analyzed by using the free software tool ImageJ.

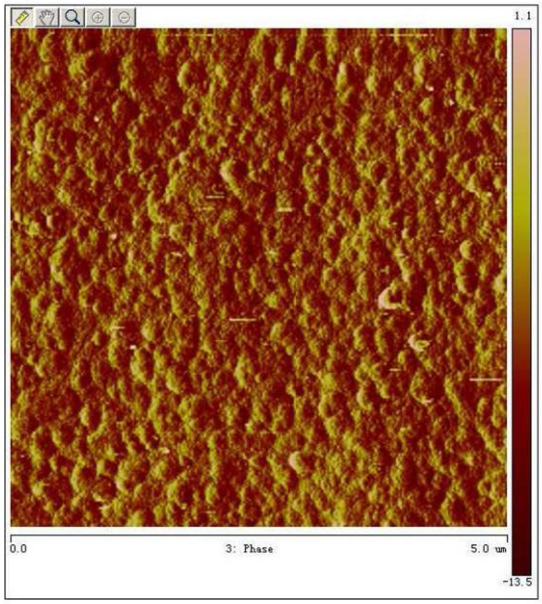

Figure S3. AFM surface profile of the rough Au layer under the TiO_2 layer. The area is 5 μm × 5 μm. The root mean squared (RMS) roughness is 11.0 nm.